RSC Advances

PAPER

View Article Online
View Journal | View Issue

Cite this: *RSC Adv.*, 2022, **12**, 11

Plasmonic enhancement of the antibacterial photodynamic efficiency of a zinc tetraphenylporphyrin photosensitizer/dextran *graft* polyacrylamide anionic copolymer/Au nanoparticles hybrid nanosystem

Oleg A. Yeshchenko, *[a] Nataliya V. Kutsevol, [b] Anastasiya V. Tomchuk, [a] Pavlo S. Khort, [a] Pavlo A. Virych, [b] Vasyl A. Chumachenko, [b] Yulia I. Kuziv, [b] Antonina P. Naumenko [a] and Andrey I. Marinin [c]

A zinc tetraphenylporphyrin photosensitizer/dextran *graft* polyacrylamide anionic copolymer/Au nanoparticles (ZnTPP/D-*g*-PAAan/AuNPs) triple hybrid nanosystem was synthesized in water-based solution as a nanodrug for potential photodynamic therapy applications. Dynamic light scattering studies showed that the nanosystem is stable against aggregation and sedimentation for several days after preparation. The dependence of the ZnTPP fluorescence intensity on the gold concentration in the ZnTPP/D-*g*-PAAan/AuNPs nanosystem has been revealed to be non-monotonic, with a maximum 2.5-fold enhancement at a concentration of 0.008 g L^{-1}. The non-monotonic dependence was explained to be caused by two competing processes, namely plasmonic enhancement and FRET, indicating the existence of an optimal concentration of Au NPs that can provide the highest plasmonic enhancement of the electronic processes involving the ZnTPP photosensitizer. A 2.6-fold enhancement of singlet oxygen photogeneration under excitation resonant with the localized surface plasmon resonance of the Au NPs has been detected for ZnTPP/D-*g*-PAAan/AuNPs, proving the plasmonic origin of this phenomenon. The high bactericidal efficiency of ZnTPP/D-*g*-PAAan/AuNPs water-based solution under 420 nm and 530 nm light irradiation was revealed against wild strains of *Staphylococcus aureus*. Therefore, the ZnTPP/D-*g*-PAAan/AuNPs nanosystem can potentially be used in photodynamic therapy for the prevention and treatment of the bacterial contamination of open wounds.

Received 8th November 2021
Accepted 7th December 2021

DOI: 10.1039/d1ra08198e

rsc.li/rsc-advances

1. Introduction

In 2014, the World Health Organization warned of the inevitability of a "post-antibiotic era" caused by the growing resistance of bacteria to many antibiotics in recent years and the emergence of multidrug-resistant bacteria.[1] Thus, great attention has been directed towards alternative antibacterial therapies, such as antibacterial photodynamic therapy (APDT). APDT is based on utilizing light and a light-sensitive agent, a photosensitizer (PS), and it is usually applied in an oxygen-rich environment.[2,3] Recent research has proved that APDT can be an efficient alternative to the use of antibiotics and has some advantages: the antibacterial effect is independent of antibiotic resistance, the harmful effects on host tissue are more limited, and there is no resistance after multiple session of APDT. The mechanism of action of APDT is based on the use of a PS, which can produce cytotoxic singlet oxygen and free radicals after irradiation at a certain wavelength. Singlet oxygen and free radicals have a deadly effect on microorganisms.[4]

Now a days, the most efficient PSs applied in photodynamic therapy (PDT) are based on porphyrin and its derivatives.[5,6] The advantages of porphyrins as PSs include their stability, efficient absorption of visible light, high yields of singlet oxygen, easy functional modification, long triplet-state lifetimes, and low dark toxicity. However, almost all PSs are hydrophobic, causing their aggregation in biological environments and resulting in a reduction in photochemical efficacy.[6] Metal-porphyrins have attracted considerable attention over the last few years. The PDT activity of a metal complex depends on the exact metal due to paramagnetic effects.[7] To increase the stability of the porphyrin ring and to maintain the photophysical properties of the PS, zinc can be added into the porphyrin ring. Such structures, *e.g.*, zinc tetraphenylporphyrin (ZnTPP), are more similar to natural

[a]*Physics Department, Taras Shevchenko National University of Kyiv, 60 Volodymyrska str., 01601 Kyiv, Ukraine. E-mail: yes@univ.kiev.ua*

[b]*Chemistry Department, Taras Shevchenko National University of Kyiv, 60 Volodymyrska str., 01601 Kyiv, Ukraine*

[c]*Problem Research Laboratory, National University of Food Technology, 68 Volodymyrska str., 01601 Kyiv, Ukraine*

porphyrin in comparison with *meso*-substituted porphyrins and they have been widely used in biological studies. It was reported that the presence of zinc in the porphyrin ring reduced mitochondrial binding and promoted membrane binding due to complexation with phospholipid phosphate groups, resulting in an increase in the photodynamic effect.[8]

Recently, several gold-based compounds have been synthesized, and their high anticancer efficacy was demonstrated.[9,10] In addition, gold nanoparticles (AuNPs) are used for numerous biological applications. They have lower toxicity compared to silver NPs.[11,12] In addition, a promising approach is to use Au NPs in addition to localized surface plasmon resonance (LSPR). This phenomenon, in which the free electrons in metal NPs oscillate collectively when irradiated with light resonant with the LSPR frequency, causes a frequency-dependent plasmonic enhancement effect. Excitation of the LSPR of metal NPs leads to the formation of an enhanced local electric field close to the surface of the NPs. This strong local electric field enhances the optical processes in molecules functionalized on the surface of the metal NPs or close to a rough metal surface, namely Raman scattering (SERS), absorption (SEIRA), fluorescence (SEF), photocatalysis, *etc.*13–15 The plasmonic enhancement of light absorption by PS molecules located near the surface of metal NPs in a hybrid nanosystem should lead to more effective singlet oxygen production and, hence, to enhanced PDT efficiencies in such nanosystems.[16–20] Also, it has been reported[21] that Au NPs induce antibacterial activity against some pathological bacteria due to their ultra-fine size, which facilitates cellular penetration. In addition, the antibacterial activity of Au NPs might be improved by the generation of reactive oxygen, increasing the oxidative stress faced by microbial cells. Another plasmon-originating phenomenon which can be useful for PDT purposes is the photothermal effect, or so-called plasmonic heating. This heating effect has resonant character; namely, the heating becomes especially strong when the frequency of the incident light is close to the LSPR frequency, as reported in our recent studies.[22–24] Since metal NPs have very low light emission quantum yields, almost all the absorbed light energy is converted to heat energy. Correspondingly, the NPs serve as highly efficient localized heat sources on the nanometer length-scale. Therefore, plasmonic heating makes metal NPs useful for photothermal therapy applications for targeting cancer and for antibacterial treatment.[25–28] It has been proved that the therapeutic effects were enhanced due to the photothermal degradation of the relevant cells. Thus, Au NPs combined with laser exposure can be used as an effective antibacterial approach.

Polymeric nanomaterials have become a prominent biomedical research area. The application of biocompatible water-soluble polymers in nanomedicine can improve the bioavailability, pharmacokinetics, and, therefore, effectiveness of therapeutic agents.[29] Polymers can be efficient matrices for the *in situ* synthesis of metal NPs, preventing their aggregation and allowing the nanoparticle size to be regulated.[30–33] The multifunctionality of polymer molecules, with unique chemical and biological properties, allows the controlled delivery and release of various therapeutic agents. They are stable in the body, can provide optimal pharmacokinetics and biodistribution, can ensure the protection of healthy tissues, and can support accumulation of drugs in diseased tissue. Partially, the encapsulation of PSs into a polymer matrix allows the aggregation of hydrophobic molecules of dye to be avoided and drastically increases the PDT efficacy in a biological environment.[34]

In the present paper we have focused on the synthesis and study of the morphology, optical properties, and antibacterial activity of a water solution of a triple hybrid ZnTPP/D-*g*-PAAan/AuNPs composite nanosystem consisting of a zinc tetraphenylporphyrin (ZnTPP) photosensitizer, an anionic form of a dextran polyacrylamide *graft* copolymer (D-*g*-PAAan), and Au NPs. The potential use of the ZnTPP/D-*g*-PAAan/AuNPs nanosystem for PDT applications has been analyzed. The features of the binding of ZnTPP molecules to D-*g*-PAAan/AuNPs macromolecules and their interactions with the D-*g*-PAAan polymer and gold NPs have been studied. The essential effects of Au NP LSPR on the light absorption and fluorescence of ZnTPP molecules, on singlet oxygen generation, and, correspondingly, on the antibacterial activity of the ZnTPP/D-*g*-PAAan/AuNPs hybrid nanosystem have been revealed. The high potential of ZnTPP/D-*g*-PAAan/AuNPs for the rapid antibacterial PDT of open wounds has been concluded.

Usually, for the prevention and treatment of the bacterial contamination of open wounds, conventional antibacterial agents like ethanol and povidone iodine are widely used. However, while ethanol is used as an antiseptic for minor skin damage, for large wounds, it is unsuitable due to the possibility of additional tissue damage and dehydration. Such processes kill bacteria but also prevent tissue regeneration. Another disadvantage of such antiseptics is the need for their periodic addition to the wound. The use of aqueous polymer systems with NPs of gold or silver provides long-lasting antibacterial effects due to the gradual release of active ingredients into the wound environment. The use of a three-component system with a photosensitizer and Au NPs after irradiation with light can quickly reduce the colony-forming unit (CFU) number of bacteria. The presence of NPs provides prolonged antibacterial effects. We have previously conducted similar studies using chlorhexidine, miramistin, antibiotics, and silver NPs.[35–38] The aim of these studies was to identify the presence and features of the antibacterial activities of two and three-component systems *in vitro* and the possibility of their use in PDT. Under such conditions, it makes no sense to use classic antiseptics such as ethanol or povidone iodine. In the future, we plan to study such three-component systems using animal models and compare the results with classical methods for the decontamination of open wounds, systems with silver NPs, and classical PDT methods (*e.g.*, methylene blue), including studying the effects against drug-resistant strains of *Staphylococcus aureus* and *Pseudomonas aeruginosa*.

2. Experimental

2.1 The fabrication of ZnTPP/D-*g*-PAAan and ZnTPP/D-*g*-PAAan/AuNPs hybrid nanosystems

The nanosystem was prepared using a polymer matrix of a star-like dextran-*graft*-polyacrylamide copolymer in anionic form (D-

g-PAAan). For the synthesis of the initial non-charged copolymer, dextran with a molecular weight (M_w) of 7×10^4 (Fluka) and acrylamide (Aldrich) were used. Cerium(IV) ammonium nitrate (Aldrich) was the initiator for radical polymerization. The number of grafting sites per dextran backbone was predetermined based on the molar ratio of acrylamide to cerium ions and it was equal to 5. Details of the synthesis and characterization of the copolymer have been described elsewhere,[39] and the molecular parameters of this copolymer are shown in Table 1, where M_w is the weight average molecular weight, R_g is the radius of gyration, and M_w/M_n is the polydispersity index.

The anionic form of this copolymer (referred to throughout as D-*g*-PAAan) was obtained *via* the alkaline hydrolysis of the initial *graft* copolymer for 30 min using 0.25 M NaOH. Alkaline hydrolysis leads to the conversion of the $-CONH_2$ groups of the PAA chains to –COONa groups, as shown in Fig. 1. The amount of carboxylated groups in the modified copolymer macromolecules was determined *via* potentiometric titration, and the degree of hydrolysis was equal to 37%. It has been proven that the selected hydrolysis conditions do not lead to the destruction of the macromolecules.[40] The obtained anionic copolymer was purified by means of precipitation with acetone, then freeze-dried and kept in a vacuum desiccator to prevent further hydrolysis. All polymer solutions for further investigations were prepared in double-distilled water. It was shown that the synthesized polymer was star-like; its macromolecular structure was more rigid in comparison with linear PAA. The star-like copolymer in anionic form has a more rigid and expanded structure compared to its non-charged analogue. It has been demonstrated that branched polymer matrices are more efficient for the *in situ* synthesis of metal nanoparticles.[31,41]

Au NPs were synthesized *via* the reduction of the Au precursor ($HAuCl_4$) dissolved in polymer solution. 0.05 mL of 0.1 M $HAuCl_4$ aqueous solution was added to 1 mL of water polymer solution ($c = 1$ g L^{-1}) and stirred for 20 min. Then, 0.1 mL of 0.1 M aqueous $NaBH_4$ solution was added. The final solution was stirred for 30 min. It turned ruby-red in color, indicating the formation of Au NPs.

Zinc tetraphenylporphyrin (ZnTPP) was dissolved in ethanol at 40 °C. As a result, a stock solution of ZnTPP in ethanol with a concentration of 0.1 g L^{-1} was obtained. Stock solutions of D-*g*-PAAan ($c = 1$ g L^{-1}) and D-*g*-PAAan/AuNPs ($c_{D\text{-}g\text{-}PAAan} = 0.8696$ g L^{-1} and $c_{Au} = 0.8565$ g L^{-1}) were diluted in water at room temperature to prepare diluted solutions with various concentrations. Then, 0.03 mL of ZnTPP ethanol solution ($c = 0.1$ g L^{-1}) was added to 2.97 mL of the diluted solutions of D-*g*-PAAan and D-*g*-PAAan/AuNPs. The concentration of ZnTPP in the obtained ZnTPP/D-*g*-PAAan and ZnTPP/D-*g*-PAAan/AuNPs nanosystems was constant and equal to 0.001 g L^{-1}. The concentrations of D-*g*-PAAan and/or Au NPs varied.

Table 1 The molecular parameters of the D-*g*-PAAan copolymer, as determined *via* size exclusion chromatography

Sample	M_w (x 10^{-6})	Rg (nm)	M_w/M_n
D-*g*-PAAan	2.15	85	1.72

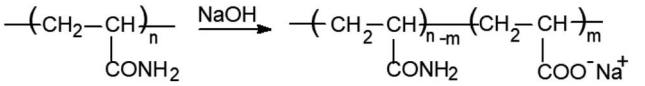

Fig. 1 The alkaline-hydrolysis-based transformation of the non-charged D-*g*-PAA copolymer to the charged anionic D-*g*-PAAan form.

2.2 Optical characterization

The intensity-weighted hydrodynamic particle size distributions (PSDs) in water solution were determined *via* dynamic light scattering (DLS) using Zetasizer Nano-ZS90 apparatus (Malvern Panalytical). The instrument was equipped with a He–Ne laser (5 mW) operating at a wavelength of 633 nm. The scattering angle was 173°. PSDs were estimated from autocorrelation functions using the nonnegative truncated singular value decomposition method, as has been described elsewhere.[42] The DLS measurements were performed at room temperature.

The absorption spectra were recorded using a Cary 60 UV-VIS spectrophotometer (Agilent Technologies Inc.). The fluorescence (FL) spectra were recorded using a Shimadzu RF-6000 spectrofluorophotometer (Shimadzu Corp.) with a wavelength of 421 nm for FL excitation. The singlet oxygen emission spectra were recorded with a FluoroMax Plus CP spectrofluorometer (HORIBA Scientific) at wavelengths of 421 and 553 nm for the excitation of singlet oxygen emission. Solution samples were placed in a 1 cm × 1 cm × 4 cm polished quartz cell. The spectra were measured at room temperature. The measurements were carried out with time delays from 1 min to 7 days after the mixing of ZnTPP ethanol solution with water and water-based solutions of D-*g*-PAAan and D-*g*-PAAan/AuNPs.

2.3 Biological experiments

Staphylococcus aureus (*S. aureus*) was isolated from open wounds on yolk-salt agar with the following composition (g L^{-1}): peptone, 10; sodium chloride, 70; heart extract powder, 5; mannitol, 15; and agar, 15, and the pH was 7.3. The sensitivity of *S. aureus* to the actions of the different types of nanosystems (D-*g*-PAAan, D-*g*-PAAan/AuNPs, ZnTPP/D-*g*-PAAan, and ZnTPP/D-*g*-PAAan/AuNPs) was determined in a Mueller-Hinton liquid environment with the following composition (g L^{-1}): casein hydrolysate, 17.5; peptone, 2; and water-soluble starch, 1.5, and the pH was 7.3. The final CFU number in suspension was 3–4 × 10^6 per ml. The bacterial suspension was divided into 1 mL aliquots and was incubated in a water bath at 37 °C throughout the experiments. Before adding the nanosystem test samples, the *S. aureus* suspensions were incubated for 20 min at 37 °C to adapt to the experimental conditions. The toxicity levels of the individual components of the hybrid nanosystem were tested. Cytotoxicity measurements were performed at 5 min intervals for 30 min. The final concentration of ZnTPP was equal to 0.001 g L^{-1}, and the final concentrations of D-*g*-PAAan and Au NPs were 0.08, 0.008, and 0.0008 g L^{-1}. Changes in the number of CFUs were evaluated relative to a bacterial suspension that was kept under similar conditions but without the addition of nanosystems.

A LIKA-LED medical light therapy LED device (Photonica Plus) was used for light irradiation (420 and 530 nm). The light power was 0.1 J s^{-1}, and the irradiation dose was raised from 3 to 18 J mL^{-1} at increments of 3 J mL^{-1}. The suspension was irradiated for 15 min after adding the solution. The number of CFUs was calculated in a Goryaev chamber after suspension staining with acridine orange (3.5×10^{-3} M). Mathematical and statistical processing of the obtained results was performed using Shapiro–Wilk ($p > 0.05$) and Scheffe (ANOVA, $p < 0.05$) tests. The experiments were repeated three times.

3. Results and discussion

3.1 Dynamic light scattering

The PSDs of D-*g*-PAAan, ZnTPP, ZnTPP/D-*g*-PAAan, and ZnTPP/D-*g*-PAAan/AuNPs water-based solutions are presented in Fig. 2. DLS measurements of potentially unstable solutions (ZnTPP, ZnTPP/D-*g*-PAAan, and ZnTPP/D-*g*-PAAan/AuNPs) were performed 1 min, 1 h, 24 h, and 7 days after fabrication (mixing). The PSD of D-*g*-PAAan has a single peak at a hydrodynamic radius (R_H) of 42 nm (Fig. 2(a)). Aggregates with $R_H = 32$ nm were observed in the case of ZnTPP due to its poor solubility in water (Fig. 2(b), black line).

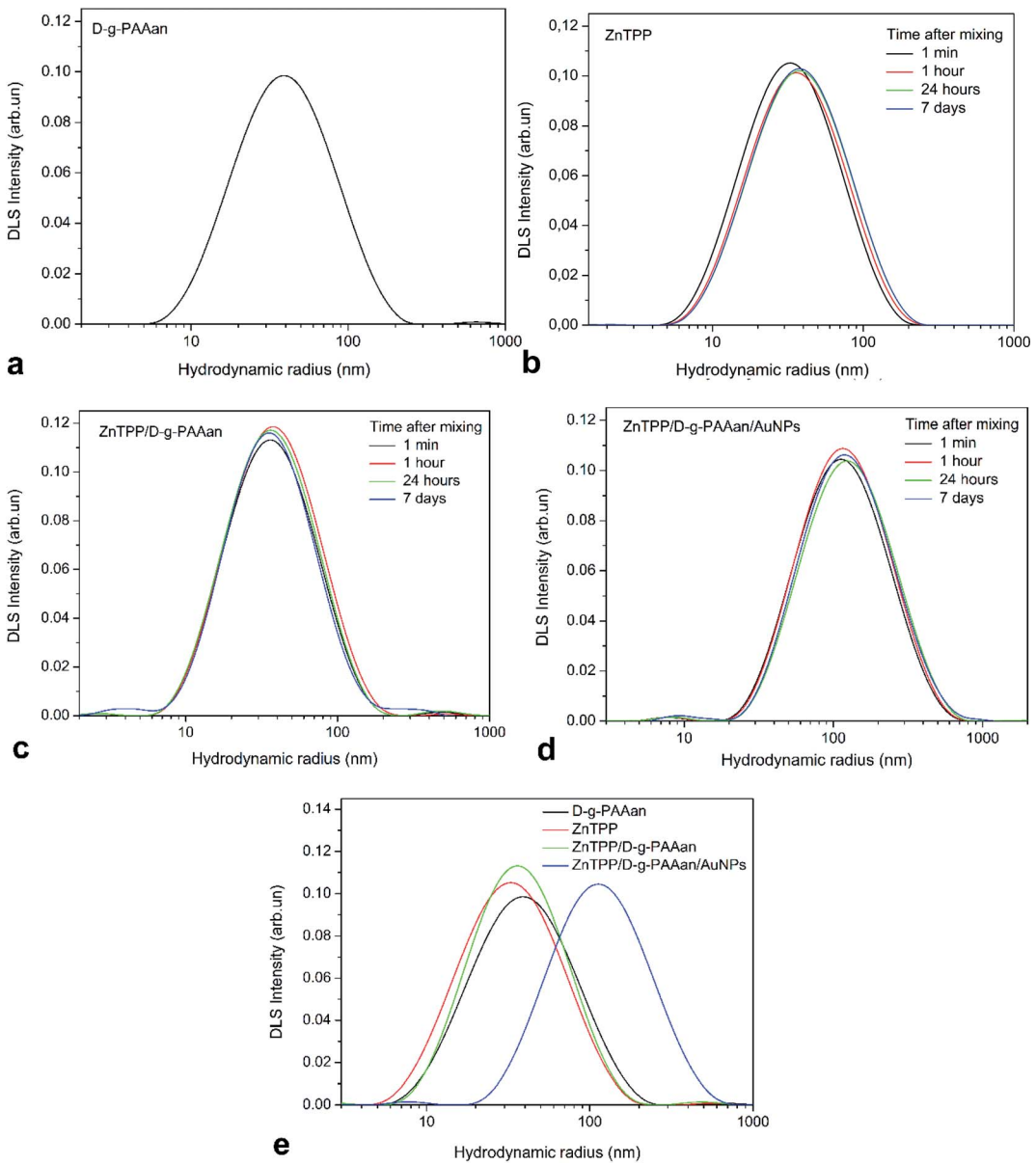

Fig. 2 (a) The PSD of D-*g*-PAAan water solution. PSDs of freshly prepared (1 min) water-based solutions and these solutions after 1 h, 24 h, and 7 days: (b) ZnTPP, (c) ZnTPP/D-*g*-PAAan, and (d) ZnTPP/D-*g*-PAAan/AuNPs. (e) PSDs of freshly prepared D-*g*-PAAan, ZnTPP, ZnTPP/D-*g*-PAAan, and ZnTPP/D-*g*-PAAan/AuNPs in water.

As it is shown in Fig. 2(b), the PSD of ZnTPP water-based solution did not significantly change during the observed period of time. Only after 7 days did the peak slightly shift to a higher hydrodynamic radius value. A mixture of ZnTPP and D-*g*-PAAan has a PSD similar to free D-*g*-PAAan and ZnTPP, with a peak maximum at 38 nm (Fig. 2(c), black line), which is expected taking into account the close R_H values of the individual solution components. Also, ZnTPP/D-*g*-PAAan appeared to be stable against aggregation and sedimentation, with R_H values of 38–41 nm over the observed period. It should be noted that insignificant aggregation was observed for this system over 24 h. Unexpectedly, an additional fraction of small particles (R_H = 4 nm) was observed after 7 days.

The PSD of the three-component ZnTPP/D-*g*-PAAan/AuNPs nanosystem has two peaks at R_H = 8 nm and at R_H = 116 nm (Fig. 2(d), black line). The first maximum corresponded to Au NPs and the second one to the ZnTPP/D-*g*-PAAan/AuNPs hybrid nanosystem. It should be noted that despite the low intensity of the Au NPs peak in the intensity-weighted PSD, the relative number of Au NPs is very high since, according to Rayleigh scattering theory, the intensity of small particle scattering is directly proportional to R_H^6. We observed no change in the PSD of the ZnTPP/D-*g*-PAAan/AuNPs system during the first 7 days after preparation (Fig. 2(d), red, green, and blue curves). The PSDs of all systems discussed in the current paper are shown in Fig. 2(e) to facilitate a direct comparison.

3.2 Absorption and fluorescence spectroscopy

3.2.1 Spectra transformations due to the binding of ZnTPP to D-*g*-PAAan and D-*g*-PAAan/AuNPs. Absorption spectroscopy measurements were performed with the PS ZnTPP in ethanol as a reference, and analysis of ZnTPP mixed with water and water-based solutions of the D-*g*-PAAan polymer and D-*g*-PAAan/AuNPs hybrid nanosystem was carried out, as shown in Fig. 3. The absorption spectrum of ZnTPP in ethanol (Fig. 3(a), black line) has the typical structure of a porphyrin in an organic solvent. Namely, there are weak long-wavelength (530–620 nm) Q bands and strong short-wavelength (380–440 nm) B (Soret) bands originating from $S_0 \rightarrow S_1$ and $S_0 \rightarrow S_2$ transitions from the π electron ground state to the 1st and 2nd excited π electron states of the porphyrin molecules, respectively.[43–46] The Q and B bands have a multicomponent structure, reflecting the vibrational structure of the excited electron states. The $S_0 \rightarrow S_1$ transition is weakly allowed and the $S_0 \rightarrow S_2$ transition is strongly allowed by selection rules, causing the low intensity of the Q bands and the high intensity of the B band in the spectrum. Meanwhile, the absorption spectrum of the D-*g*-PAAan/AuNPs hybrid system shows a clear LSPR band from Au NPs centered at 520 nm, as seen in Fig. 3(b) (orange line). The absorption and FL spectra of the D-*g*-PAAan polymer are located in the UV range, out of the spectral range studied in the present work.

Mixing ZnTPP ethanol solution with water leads to essential changes in the intensity and shape of the absorption spectrum, as seen in Fig. 3(a) (blue line). In Fig. 3(a), the spectra are normalized by intensity to see better the changes in the shape of the spectra occurring upon mixing. The total intensity of the B band decreases sharply (2.5-fold). Simultaneously, the B band broadens greatly and its doublet structure disappears. Meanwhile, the relative intensity of the weak Q bands increases. Since ZnTPP is insoluble in water, it is most probably that the absorption spectrum transformation is due to the aggregation of hydrophobic ZnTPP molecules in the aqueous environment. This assumption of ZnTPP aggregation is in full agreement with DLS data, revealing the existence of aggregates of ZnTPP molecules with a radius of 32 nm radius in water. Mixing an ethanol solution of ZnTPP with water solutions of D-*g*-PAAan and D-*g*-PAAan/AuNPs does not lead to any remarkable changes in the absorption spectrum shape compared to the case of ZnTPP mixed with water. Since the spectra of ZnTPP and Au NPs overlap considerably, to better observe the transformation of the ZnTPP spectrum upon mixing, we analyzed the difference spectrum of ZnTPP/D-*g*-PAAan/AuNPs and D-*g*-PAAan/AuNPs, as shown in Fig. 3(a) and (b) (red lines).

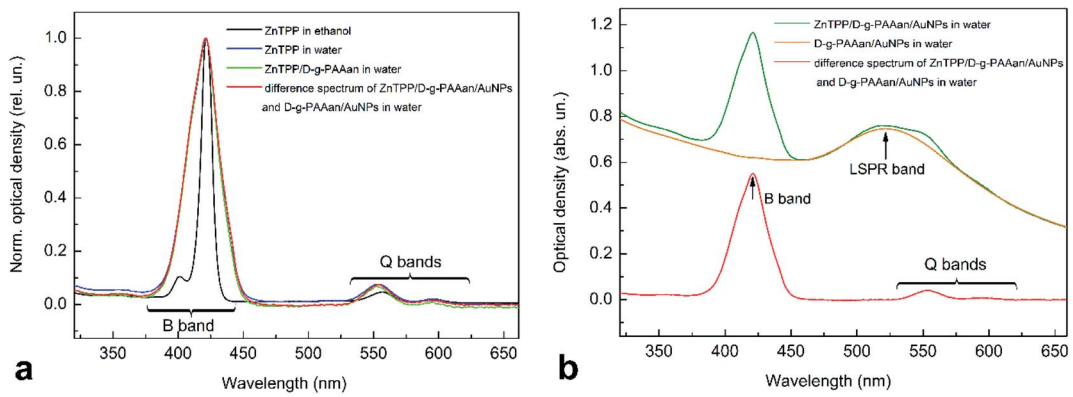

Fig. 3 (a) Normalized absorption spectra of ZnTPP in ethanol and ZnTPP in ethanol mixed with water and D-*g*-PAAan water-based solution, and the difference spectrum between ZnTPP/D-*g*-PAAan/AuNPs and D-*g*-PAAan/AuNPs solutions. (b) Normalized absorption spectra of ZnTPP/D-*g*-PAAan/AuNPs and D-*g*-PAAan/AuNPs solution and the difference spectrum between ZnTPP/D-*g*-PAAan/AuNPs and D-*g*-PAAan/AuNPs solutions. The difference spectrum is presented to subtract Au NP absorption. The concentrations were as follows: ZnTPP, 0.001 g L^{-1}; D-*g*-PAAan, 0.080 g L^{-1}; Au, 0.079 g L^{-1}.

The FL spectra were measured for ZnTPP in ethanol and for mixtures of ZnTPP in ethanol with water and water-based solutions of D-*g*-PAAan and D-*g*-PAAan/AuNPs, as shown in Fig. 4. The FL spectrum of ZnTPP in ethanol (Fig. 4, black line) shows the typical structure for a porphyrin in an organic solvent. Namely, two bands dominate the spectrum: the short-wavelength (602 nm) and long-wavelength (655 nm) bands, depicted as F_{00} and F_{01}, respectively. The F_{00} and F_{01} bands originate from $S_1(0) \rightarrow S_0(0)$ and $S_1(0) \rightarrow S_0(1)$ radiative transitions from the ground vibrational level of the 1st excited π electron state to the ground and 1st excited vibrational levels of the ground π electron state of the porphyrin molecule, respectively.[44,45]

Similar to the changes in the absorption spectrum, mixing ZnTPP with water results in clear changes in the intensity and shape of the FL spectrum, as seen in Fig. 4 (blue line). In Fig. 4, the spectra are normalized by intensity to see better the changes in the shape of spectra occurring upon mixing. The total FL intensity is quenched sharply, 8.5-fold. The F_{00} band intensity decreases considerably relative to the intensity of the F_{01} band. The F_{01} band red shifts by 9 nm. Since ZnTPP is insoluble in water, as is noted above, it is most probable that the observed changes in the FL spectrum are due to the aggregation of hydrophobic ZnTPP molecules in the aqueous environment. Next, mixing ZnTPP with D-*g*-PAAan polymer water-based solution leads to a further decrease in the F_{00} band intensity comparing to the case of ZnTPP mixed with water, as seen in Fig. 4 (green line). Finally, the red line in Fig. 4 shows the FL spectrum of ZnTPP mixed with D-*g*-PAAan/AuNPs water-based solution. It is seen that the FL spectrum of ZnTPP/D-*g*-PAAan/AuNPs is transformed compared to the case of ZnTPP in ethanol, but these transformations are essentially weaker than the ones seen for ZnTPP in water and ZnTPP in D-*g*-PAAan water-based solution. Thus, the FL spectrum transformations differ from each other for ZnTPP in water and in D-*g*-PAAan and D-*g*-PAAan/AuNPs water-based solutions. Correspondingly, proceeding from the FL data, one can conclude that ZnTPP molecules interact with D-*g*-PAAan and D-*g*-PAAan/AuNPs macromolecules, and that the interactions are different in the presence and absence of Au NPs.

The assumption of binding between ZnTPP molecules and D-*g*-PAAan and D-*g*-PAAan/AuNPs macromolecules was checked directly *via* measuring the FL anisotropy factor *r*, which characterizes the degree of freedom of molecules during their motion. The anisotropy factor for ZnTPP in ethanol was measured to be 0.7%, which shows the free motion of ZnTPP in ethanol. However, for ZnTPP in water, the value of *r* was measured to be 10%, which indicates a decrease in the degree of motion of ZnTPP molecules due to their hydrophobic interactions with the aqueous environment. The mixing of ZnTPP with D-*g*-PAAan water-based solution leads to a further increase of the FL anisotropy factor (20%), which proves the binding of ZnTPP molecules to polymer macromolecules. Finally, the *r* factor value for ZnTPP mixed with D-*g*-PAAan/AuNPs water-based solution was measured to be 36%, indicating that ZnTPP molecules bind most strongly with hybrid macromolecules containing Au NPs. The *r* factor measurements were performed at the following concentrations: ZnTPP, 0.001 g L^{-1}; D-*g*-PAAan, 0.080 g L^{-1}; Au, 0.079 g L^{-1}.

3.2.2 The temporal behavior of the FL spectra of ZnTPP/D-*g*-PAAan and ZnTPP/D-*g*-PAAan/AuNPs systems. The behavior of the total FL intensity of ZnTPP as time elapsed after mixing ZnTPP in ethanol with water and water-based solutions of D-*g*-PAAan and D-*g*-PAAan/AuNPs was studied. The obtained results are presented in Fig. 5. It is seen that the FL intensity decreases with time monotonically for ZnTPP in water (Fig. 5, triangles) to 0.31, 7 days after mixing, compared with the initial value. This FL quenching is due to the oxidation of the ZnTPP molecules. Meanwhile, the mixing of ZnTPP with D-*g*-PAAan (Fig. 5,

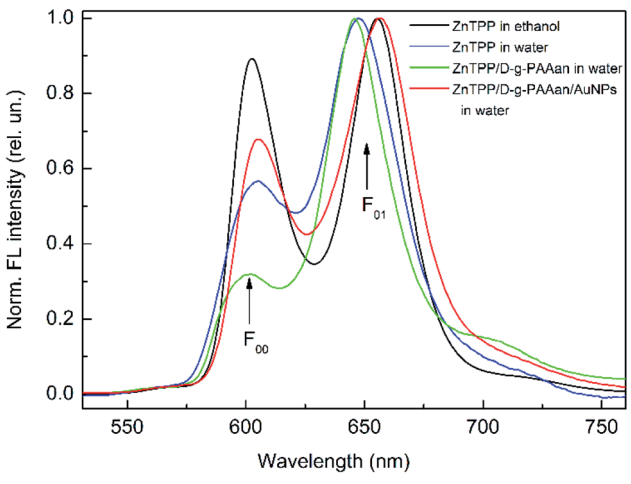

Fig. 4 Normalized fluorescence spectra of ZnTPP in ethanol and ZnTPP in ethanol mixed with water, D-*g*-PAAan water-based solution, and D-*g*-PAAan/AuNPs water-based solution; excitation: 421 nm; concentrations: ZnTPP, 0.001 g L^{-1}; D-*g*-PAAan, 0.080 g L^{-1}; Au, 0.079 g L^{-1}.

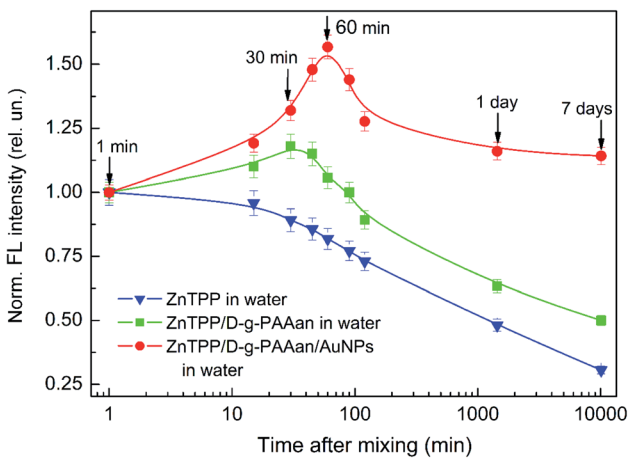

Fig. 5 The dependence of the normalized FL intensity of ZnTPP on time after mixing with D-*g*-PAAan water-based solution (squares) and D-*g*-PAAan/AuNPs water-based solution (circles). The FL intensities are normalized to the respective values 1 min after mixing. The concentrations are as follows: ZnTPP, 0.001 g L^{-1}; D-*g*-PAAan, 0.080 g L^{-1}; Au, 0.079 g L^{-1}. The experimental points are spline-interpolated for convenience.

squares) and D-*g*-PAAan/AuNPs (Fig. 5, circles) water-based solutions initially leads to an increase in the FL intensity, which then is changed to a decrease, similar to what is observed for ZnTPP in water. It is quite reasonable to assume that the initial FL intensity increase is caused by the binding of ZnTPP molecules to D-*g*-PAAan and D-*g*-PAAan/AuNPs macromolecules. On the 7th day after mixing, the ZnTPP/D-*g*-PAAan FL intensity is 0.5 and the ZnTPP/D-*g*-PAAan/AuNPs FL intensity is 1.14 compared to the initial values just (1 min) after mixing. It should be noted that on the 7th day after mixing, the FL intensities of ZnTPP bound to ZnTPP/D-*g*-PAAan and ZnTPP/D-*g*-PAAan/AuNPs macromolecules are higher than that of free ZnTPP in water. Thus, one can conclude that the D-*g*-PAAan and D-*g*-PAAan/AuNPs macromolecules protect the ZnTPP molecules bound to them from oxidation. Moreover, taking into account that the duration of the FL intensity increase for ZnTPP/D-*g*-PAAan/AuNPs (about 60 min) is larger than for ZnTPP/D-*g*-PAAan (about 30 min) and that the FL intensity 7 days after mixing is considerably higher for ZnTPP/D-*g*-PAAan/AuNPs than for ZnTPP/D-*g*-PAAan, one can conclude that the presence of the Au-NP-based nanosystem provides significantly higher efficiency when it comes to protecting the photosensitizer molecules from oxidation. The additional cause of the long-lasting intense FL of ZnTPP bound to D-*g*-PAAan/AuNPs macromolecules is the enhancement of FL in the plasmonic field of the Au NPs due to the close spatial separation of the ZnTPP molecules and Au NPs in the inner volume of the hybrid polymer macromolecules.

3.2.3 Concentration effects on the fluorescence of ZnTPP/D-*g*-PAAan and ZnTPP/D-*g*-PAAan/AuNPs systems. Studying the influence of variations of the concentrations of the PS, polymer, and Au NPs on the optical properties of the hybrid nanosystem is very important for understanding the impact of ZnTPP interactions with the polymer and Au NPs on the electronic processes relating to ZnTPP molecules in the hybrid nanosystem. Initially, we studied the impact of the ZnTPP concentration on the FL intensity in ethanol solution and in a mixture with water, as shown in Fig. 6. It is seen that the dependence of the FL intensity of ZnTPP in ethanol (squares) is non-monotonic; the FL intensity increases with increasing concentration, reaches a maximum at 0.005 g L^{-1}, and then decreases with a further increase in concentration. Evidently, the observed non-monotonic dependence is caused by the aggregation of ZnTPP molecules at high concentrations. Similar to ethanol solution, the concentration dependence of the FL intensity of ZnTPP in an ethanol mixture with water is also non-monotonic, with a maximum at a lower concentration of 0.0025 g L^{-1}. The lower value of the concentration-dependent maximum for ZnTPP in water is due to the hydrophobicity of ZnTPP molecules, enforcing their aggregation at lower concentrations. Therefore, a ZnTPP concentration of 0.001 g L^{-1} was chosen for further experiments. This value lies in the center of the linear area of the increasing FL trend, corresponding to a quite low concentration at which no aggregation occurs.

Next, we studied the impact of varying the concentrations of the polymer and Au NPs on the total FL intensity of ZnTPP in ZnTPP/D-*g*-PAAan and ZnTPP/D-*g*-PAAan/AuNPs nanosystems, as shown in Fig. 7. The FL intensities at various concentrations were normalized with respect to the FL intensity of ZnTPP in water. Since the ZnTPP FL spectrum and Au NP absorption spectrum have sufficient spectral overlap (Fig. 3(b) and 4), the Au NPs partially reabsorb fluorescence photons emitted by ZnTPP molecules. Correspondingly, the measured FL intensity $I(\lambda)$ could be described using the relationship $I(\lambda) = I_0(\lambda)10^{-D(\lambda)}$,

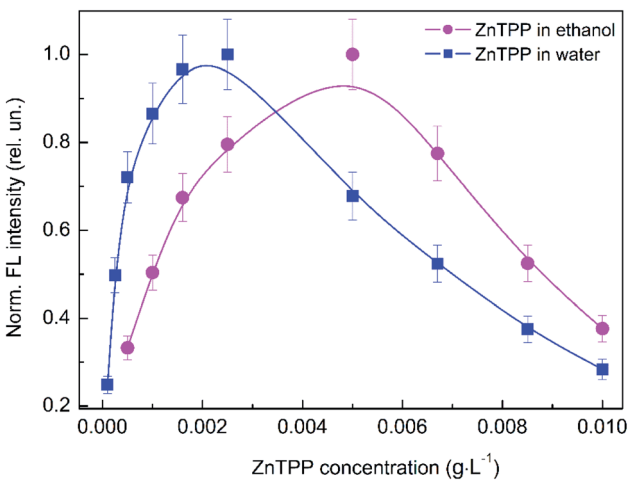

Fig. 6 The dependence of the normalized total fluorescence intensity on the ZnTPP concentration for ZnTPP in ethanol and ZnTPP in ethanol mixed with water. The experimental points are spline-interpolated for convenience.

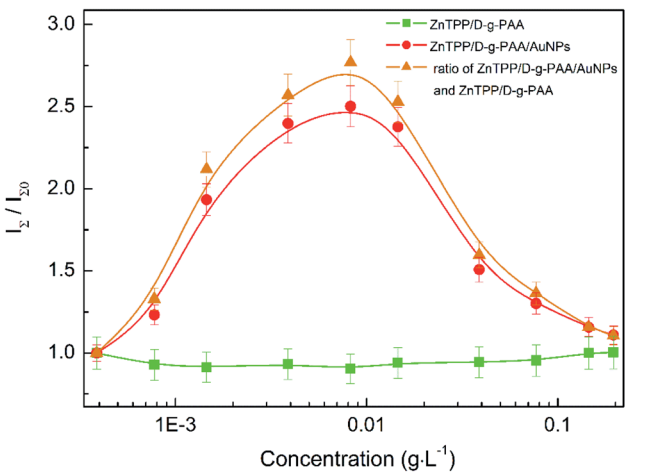

Fig. 7 The concentration dependence of the normalized total FL intensity of ZnTPP in ethanol mixed with water-based solutions of D-*g*-PAAan (squares) and D-*g*-PAAan/AuNPs (circles). The triangles show the ratio of the respective concentration dependences for ZnTPP/D-*g*-PAAan/AuNPs and ZnTPP/D-*g*-PAAan, characterizing the influence of Au NPs on the absorption and PL of ZnTPP in the triple hybrid nanosystem. The FL intensities are normalized to the respective values for ZnTPP in water. The squares present the dependence on the polymer concentration, and the circles and triangles depict the dependence on the gold concentration. ZnTPP concentration: 0.001 g L^{-1}. The experimental points are spline-interpolated for convenience.

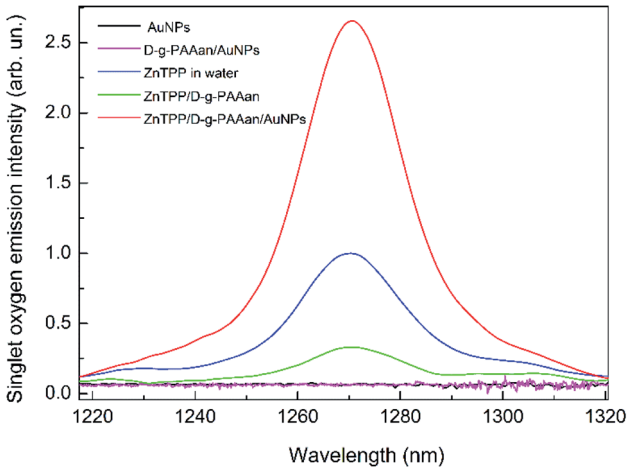

Fig. 8 Singlet oxygen emission spectra for ZnTPP in water (blue line) and ZnTPP/D-*g*-PAAan (green line) and ZnTPP/D-*g*-PAAan/AuNPs (red line) water-based solutions. Water-based solutions of Au NPs (black line) and D-*g*-PAAan/AuNPs (magenta line) without ZnTPP show no oxygen emission; excitation: 553 nm; concentrations: ZnTPP, 0.01 g L^{-1}; D-*g*-PAAan, 0.080 g L^{-1}; Au, 0.079 g L^{-1}.

where $I_0(\lambda)$ is the real FL intensity emitted by ZnTPP molecules and $D(\lambda)$ is the optical density of the studied sample associated with light absorption by Au NPs. Therefore, the real FL intensity $I_0(\lambda)$ was calculated as $I_0(\lambda) = 10^{D(\lambda)}I(\lambda)$, where all values were taken at the respective concentrations of gold. The obtained normalized concentration dependence of the FL intensity of ZnTPP bound to ZnTPP/D-*g*-PAAan/AuNPs is presented in Fig. 7 in circles.

It is seen that there is no clear dependence of the FL intensity of ZnTPP on the polymer concentration for the ZnTPP/D-*g*-PAAan system over the entire studied polymer concentration range of 0–0.2 g L^{-1}, as seen in Fig. 7 (squares). Meanwhile, the dependence of the ZnTPP FL intensity in the ZnTPP/D-*g*-PAAan/AuNPs nanosystem on the gold concentration has prominent non-monotonic character, as seen in Fig. 7 (circles). The FL intensity increases 2.5-fold in the gold concentration range of 0–0.008 g L^{-1}, reaches a maximum, and then decreases to a relative value of 1.11 with a further increase in the gold concentration to 0.2 g L^{-1}. Despite the almost-complete absence of dependence of the ZnTPP FL intensity on the polymer concentration, in order to extract the contribution of Au NPs, the concentration dependence for ZnTPP/D-*g*-PAAan/AuNPs (Fig. 7, circles) was divided by the respective values for ZnTPP/D-*g*-PAAan (Fig. 7, squares). The obtained results are shown in Fig. 7 as triangles. The FL intensity increases by 2.8-fold in the gold concentration range of 0–0.008 g L^{-1}, reaches a maximum, and then decrease to a relative value of 1.11 upon a further increase in the gold concentration to 0.2 g L^{-1}. The obtained pronounced dependence of the ZnTPP FL intensity on the gold concentration proves the close spatial location of the ZnTPP molecules and Au NPs in the volume of the D-*g*-PAAan macromolecules, which occurs due to the binding of PS molecules to D-*g*-PAAan/AuNPs macromolecules.

Let us analyze the physical mechanisms behind the impact of Au NPs on the fluorescence of the ZnTPP photosensitizer (Fig. 7, triangles). *Via* varying the concentration of Au NPs, we thereby vary the average distance between them and the ZnTPP molecules, since both the NPs and molecules are bound to the D-*g*-PAAan macromolecules. The change in distance causes a change in the strength of coupling between surface plasmons and Au NPs, with electronic excitation of the molecules.[47–52] Also, the coupling strength depends on the spectral overlap of LSPR and the electron energy levels (absorption and FL spectra) of the fluorophore (molecule). Stronger coupling takes place at smaller distances and/or with larger spectral overlap. As is noted above, in the ZnTPP/D-*g*-PAAan/AuNPs nanosystem, the ZnTPP molecules and Au NPs are located close to each other. Also, the spectral overlap between Au NP LSPR (Fig. 3(b)) and the absorption (Fig. 3) and FL (Fig. 4) spectra of ZnTPP is considerable. Therefore, it is quite reasonable to expect quite strong AuNPs–ZnTPP coupling in the studied system.

Thus, the intensity of the molecular FL is determined based on two competing physical mechanisms. The first one is plasmonic enhancement, which is stronger when the metal NP-molecule distance is smaller.[47–50,52,53] The strength of the plasmon field depends on the distance from the metal NP, as $E_{sp} \propto R^{-3}$.[52,53] The second mechanism is resonance energy transfer (RET), *via* which the energy of an excited donor (fluorophore) can be non-radiatively transferred to an acceptor (metal NP).[47–49,53,54] RET causes FL quenching. The FL quenching rate due to RET depends on the donor–acceptor distance, as $\gamma_{RET} \propto R^{-n}$.[54] There are various theoretical models through which different physical mechanisms relating to the RET phenomenon can be considered. These are Förster resonance energy transfer (FRET), nanoparticle surface-energy transfer (NSET), dipole-to-metal-particle energy transfer (DMPET), and nanoparticle-induced lifetime modification (NPILM).[54] The main difference between these RET theories is the value of n, which is in the range of $3 \leq n \leq 6$, depending on the theory. The most common RET theory is FRET, at which the energy is non-radiatively transferred through dipole–dipole coupling. The FRET efficiency depends on the donor–acceptor distance in a manner proportional to R^{-6}.[54] This effectively limits FRET to the range below 10 nm. As a result of the interplay between FL quenching due to FRET and FL enhancement due to the local plasmonic field, there exists an optimal distance between the metal NP and the fluorophore (about 10 nm) at which the FL intensity is highest.[49] At distances below 10 nm, a small decrease in the distance leads to a strong decrease in the FL intensity, *i.e.*, FL quenching. At distances larger than 10 nm, a decrease in the distance leads to an increase in the FL intensity, *i.e.*, FL enhancement.

Thus, at lower Au NP concentrations in the range of 0–0.008 g L^{-1}, the distance between ZnTPP molecules and Au NPs is too large for FRET. Therefore, an increase in the NP concentration leads to a decrease in the distance between Au NPs and ZnTPP molecules, which causes strengthening of the plasmonic enhancement of fluorescence. At concentrations of Au NPs higher than about 0.008 g L^{-1}, the NP-molecule distance becomes small enough to allow the FRET process to occur, which causes the quenching of FL with an increase of the gold concentration. Thus, one can conclude that there exists an

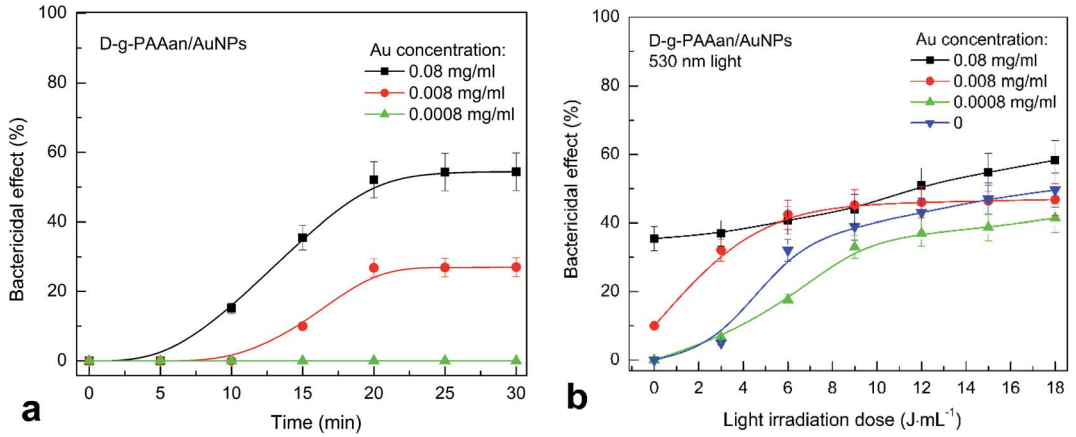

Fig. 9 The inactivation of *S. aureus* in a suspension as a function of time after adding D-*g*-PAAan/AuNPs (a) and as a function of the light irradiation dose at 530 nm (b). The blue downward-pointing triangles in (b) show the dependence obtained without adding D-*g*-PAAan/AuNPs, for reference. Concentration of Au NPs: 0.08 g L^{-1}, 0.008 g L^{-1}, and 0.0008 g L^{-1}. The light power was 0.1 J s^{-1}, and the irradiation dose was in the range of 3–18 J mL^{-1} with increments of 3 J mL^{-1}. The experimental points are spline-interpolated for convenience.

optimal concentration of Au NPs providing the highest plasmonic enhancement of the various electronic processes involving the ZnTPP photosensitizer.

3.2.4 Singlet oxygen photogeneration in the ZnTPP/D-*g*-PAAan and ZnTPP/D-*g*-PAAan/AuNPs systems. To analyze the efficiency of the ZnTPP/D-*g*-PAAan and ZnTPP/D-*g*-PAAan/AuNPs nanosystems for use in photodynamic therapy, the singlet oxygen emission spectra were measured, as shown in Fig. 8. It is seen that water-based solutions of Au NPs (black line) and D-*g*-PAAan/AuNPs (magenta line) without ZnTPP show no oxygen emission. Meanwhile, there is a clear emission peak centered at about 1270 nm, which is the characteristic wavelength of singlet O_2,[16] for ZnTPP, ZnTPP/D-*g*-PAAan, and ZnTPP/D-*g*-PAAan/AuNPs. Singlet oxygen emission was detected at excitation wavelengths of 421 nm (Soret band) and 553 nm (Q band). Under 421 nm excitation, the intensity of the emission peak is approximately the same for ZnTPP in water and for water-based solutions of ZnTPP/D-*g*-PAAan and ZnTPP/D-*g*-PAAan/AuNPs. Under 553 nm excitation, the emission intensities for ZnTPP in water and for ZnTPP/D-*g*-PAAan water-based solution are close to the respective intensities under 421 nm excitation. However, the excitation of ZnTPP/D-*g*-PAAan/AuNPs at 553 nm leads to a significant (2.6-fold) increase in the singlet oxygen emission peak intensity. Taking into account that 553 nm is close to the LSPR wavelength of Au NPs (520 nm), it is natural to suggest that the increase in the efficiency of singlet O_2 photogeneration has a plasmonic origin. Thus, plasmonic enhancement of singlet oxygen photogeneration was observed for the ZnTPP/D-*g*-PAAan/AuNPs hybrid nanosystem, showing it to be promising for use in photodynamic therapy applications.

3.3 Bactericidal photodynamic activity

It is known that the cell walls of Gram-positive bacteria consist of a thick layer of cross-linked peptidoglycans. In most microorganisms, other polymers functionalize this matrix. The presence of a significant amount of teichoic acid allows the formation of negative charge on the surface of bacterial cells. The charge of their phosphate groups is only partially compensated by crosslinked peptides and D-alanine.[55] The zeta potential of Gram-positive microorganisms is negative.[56] Nevertheless, they adhere to negatively charged surfaces and actively reproduce. Given this, it is possible to use a negatively charged polymer as a carrier for antibacterial agents.

The number of *S. aureus* CFUs in suspension after the addition of D-*g*-PAAan and ZnTPP did not change. However, the

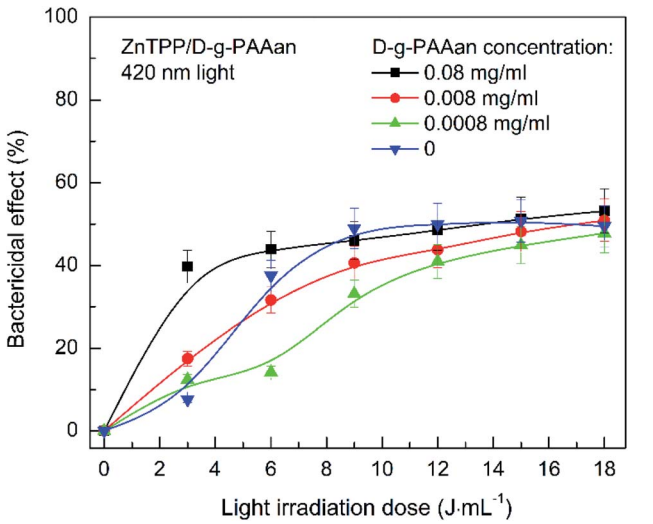

Fig. 10 The inactivation of *S. aureus* in suspensions after adding ZnTPP/D-*g*-PAAan and irradiating with 420 nm light as a function of the light irradiation dose. The blue downward-pointing triangles show the dependence without the addition of ZnTPP/D-*g*-PAAan, as a reference. Concentrations: D-*g*-PAAan: 0.08 g L^{-1}, 0.008 g L^{-1}, 0.0008 g L^{-1}; ZnTPP: 0.001 g L^{-1}. The light power was 0.1 J s^{-1} and the irradiation dose was in the range of 3–18 J mL^{-1} with increments of 3 J mL^{-1}. The experimental points are spline-interpolated for convenience.

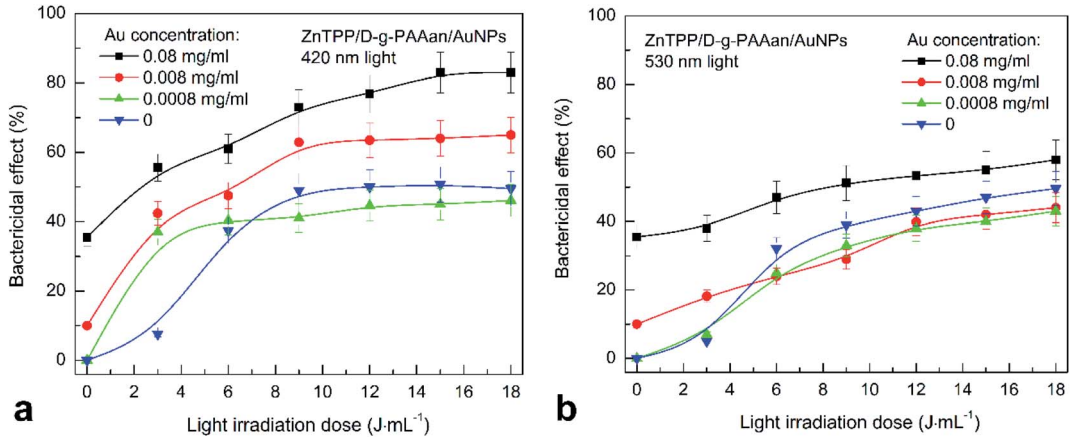

Fig. 11 The inactivation of *S. aureus* in suspension after adding ZnTPP/D-*g*-PAAan/AuNPs in combination with irradiation using 420 nm light (a) and 530 nm light (b) as a function of the irradiation dose. The blue downward-pointing triangles show the dependences obtained without adding ZnTPP/D-*g*-PAAan/AuNPs, for reference. Concentrations: Au NPs: 0.08 g L^{-1}, 0.008 g L^{-1}, and 0.0008 g L^{-1}; ZnTPP: 0.001 g L^{-1}. The light power was 0.1 J s^{-1} and the irradiation dose was in the range of 3–18 J mL^{-1} with increments of 3 J mL^{-1}. The experimental points are spline-interpolated for convenience.

numbers of CFUs of *S. aureus* in suspension are reduced by 50% and 30% within 20 min after the addition of D-*g*-PAAan/AuNPs with gold concentrations of 0.08 and 0.008 g L^{-1}, respectively (Fig. 9(a)). Meanwhile, this strain of *S. aureus* is not sensitive to D-*g*-PAAan/AuNPs with a gold concentration of 0.0008 g L^{-1}. Gold nanoparticles disrupt the normal course of biochemical processes in bacterial cells, such as DNA synthesis, ATP production, *etc.*57

Irradiation with light at 530 nm almost does not influence the antibacterial activity of D-*g*-PAAan/AuNPs with a gold concentration of 0.08 g L^{-1} (Fig. 9(b)). However, reducing the concentration 10-fold in combination with 530 nm light provides an increase in the bactericidal effect from 10% to 40% at a radiation dose of 6 J mL^{-1}. D-*g*-PAAan/AuNPs with a low gold concentration of 0.0008 g L^{-1} did not increase the efficiency under 530 nm light irradiation (Fig. 9(b)). We assume that the concentration of negatively charged polymer is important. This ensures the stability of Au NPs in solution, as well as their contact with bacterial cells. A large amount of D-*g*-PAAan polymer macromolecules provides stronger repulsion between the nanosystem and the bacteria cell walls. We assume that this is the reason for the gradual increase in the antibacterial activity over time or in response to light irradiation without the sharp increase that is characteristic of neutral polymers (Fig. 9(a) and (b)). Adding ZnTPP/D-*g*-PAAan with D-*g*-PAAan concentrations of 0.008 and 0.0008 g L^{-1} to *S. aureus* suspensions does not significantly alter the bactericidal activity under 420 nm light (Fig. 10). The number of CFUs was reduced by 40% upon the light irradiation (420 nm, 3 J mL^{-1}) of a bacterial suspension of ZnTPP/D-*g*-PAAan with a D-*g*-PAAan concentration of 0.08 g L^{-1}. Therefore, the effectiveness of ZnTPP is affected by the amount of D-*g*-PAAan.

Analysis of the bactericidal action of ZnTPP/D-*g*-PAAan/AuNPs in combination with 420 nm light irradiation showed only a gradual increase in the bactericidal effect upon increasing the irradiation dose, except at a gold concentration of 0.0008 g L^{-1} in ZnTPP/D-*g*-PAAan/AuNPs (Fig. 11(a)). The number of CFUs is linearly reduced from 50% to 20% upon increasing the irradiation dose from 3 to 18 J mL^{-1} at a gold concentration of 0.08 g L^{-1} using ZnTPP/D-*g*-PAA/AuNPs. The maximal bactericidal activity at a gold concentration of 0.008 g L^{-1} is 60% at an irradiation dose of 9 J mL^{-1}, and for a gold concentration of 0.0008 g L^{-1}, the maximum is 40% at a dose of 3 J mL^{-1}. Irradiation with 530 nm light does not contribute to any significant changes in the bactericidal activities of the nanocomposites (Fig. 11(b)).

The results indicate the significant effects of the polymer type on the bactericidal activity of the nanocomposites. A nanocontainer for bactericidal substances with a negative zeta-potential prevents the rapid interaction of the system with bacterial cells. Therefore, to achieve the maximum CFU inactivation effect, it requires more time or stimulation based on an external factor, such as light. Evidence for the gradual interaction of the polymer with bacterial cells or the slow release of the active components of the system into the environment is seen in the slight steady increase in bactericidal activity over time or with an increase in the irradiation dose. The identified effects of ZnTPP/D-*g*-PAAan/AuNPs can potentially provide a prolonged antibacterial effect after irradiation of the system with light. The obtained bactericidal activity of the nanocomposites was achieved in a short period of time, not exceeding 20 min. Therefore, the ZnTPP/D-*g*-PAAan/AuNPs nanocomposite can potentially be used for the prevention and treatment of the bacterial contamination of open wounds.

4. Conclusions

In conclusion, a ZnTPP/D-*g*-PAAan/AuNPs triple hybrid nanosystem was synthesized in water-based solution for potential use in photodynamic therapy. Anionic D-*g*-PAAan copolymer macromolecules with a dextran core and an average number of 10 PAAan grafted chains per dextran molecule were used as the

matrix for Au NPs and ZnTPP photosensitizer molecules. The ZnTPP fluorescence anisotropy factor data (ZnTPP in ethanol: 0.7%; ZnTPP in water: 10%; ZnTPP in D-*g*-PAAan water-based solution: 20%; and ZnTPP in D-*g*-PAAan/AuNPs water-based solution: 36%) proved the binding of ZnTPP molecules both with the D-*g*-PAAan polymer and D-*g*-PAAan/AuNPs hybrid macromolecules. The ZnTPP FL intensity dependence on the gold concentration was found to be non-monotonic, with a maximal 2.5-fold enhancement at a Au concentration of 0.008 g L^{-1}. The increase in intensity at low concentrations of Au NPs was explained as being a result of the enhancement of the FL of ZnTPP molecules located in the plasmonic field of the Au NPs. Meanwhile, the quenching of ZnTPP FL at higher concentrations was explained as being a result of the non-radiative FRET transfer of electronic excitation from ZnTPP molecules to Au NPs. Thus, there exists an optimal concentration of Au NPs providing the highest plasmonic enhancement of the various electronic processes involving the ZnTPP photosensitizer. A 2.6-fold surface-plasmon-mediated enhancement of singlet oxygen photogeneration under 553 nm excitation was detected for the ZnTPP/D-*g*-PAAan/AuNPs hybrid nanosystem, showing its high potential for photodynamic therapy applications. The rapid and high bactericidal efficiency of ZnTPP/D-*g*-PAAan/AuNPs water-based solution under light irradiation was revealed toward wild strains of *Staphylococcus aureus*. The observed high bactericidal efficiency was rationalized as arising due to the surface-plasmon-mediated abilities of Au NPs to enhance the singlet oxygen generation. Therefore, the ZnTPP/D-*g*-PAAan/AuNPs nanosystem can potentially be used for the prevention and treatment of the bacterial contamination of open wounds.

Author contributions

Y. K. synthesized the water-based solutions of the mentioned nanosystems. Y. K., A. T., and P. K. prepared the samples for measurements. Y. K. and A. M. performed the DLS experiments. V. C. performed the DLS data analysis and interpretation. A. T., P. K., and A. N. performed the optical measurements. P. V. performed the biological experiments. O. Y. and N. K. analyzed, interpreted, and discussed all the data, and edited the manuscript. O. Y. wrote the manuscript with input from the co-authors. O. A. and N. K. supervised the overall project.

Conflicts of interest

There are no conflicts to declare.

Acknowledgements

This work was supported by the National Research Foundation of Ukraine, Project 2020.02/0022 "Plasmon hybrid nanosystems "metal-polymer-fluorophore" with enhanced optical response for photonics and biomedical applications".

References

1 J. Ghorbani, D. Rahban, S. Aghamiri, A. Teymouri and A. Bahador, Photosensitizers in antibacterial photodynamic therapy: An overview, *Laser Ther.*, 2018, **4**, 293–302.
2 H. Abrahamse and M. R. Hamblin, New photosensitizers for photodynamic therapy, *Biochem. J.*, 2016, **473**, 347–364.
3 G. Jori, C. Fabris, M. Soncin, S. Ferro, O. Coppellotti, D. Dei, L. Fantetti, G. Chiti and G. Roncucci, Photodynamic therapy in the treatment of microbial infections: Basic principles and perspective applications, *Laser Surg. Med.*, 2006, **38**, 889–905.
4 L. Huang, Y. Xuan, Y. Koide, T. Zhiyentayev, M. Tanaka and M. R. Hamblin, Type i and Type II mechanisms of antimicrobial photodynamic therapy: An *in vitro* study on gram-negative and gram-positive bacteria, *Laser Surg. Med.*, 2012, **44**, 490.
5 A. Martinez De Pinillos Bayona, P. Mroz, C. Thunshelle and M. R. Hamblin, Design features for optimization of tetrapyrrole macrocycles as antimicrobial and anticancer photosensitizers, *Chem. Biol. Drug Des.*, 2017, **89**, 192–206.
6 Y. Lin, T. Zhou, R. Bai and Y. Xie, Chemical approaches for the enhancement of porphyrin skeleton-based photodynamic therapy, *J. Enzyme Inhib. Med. Chem.*, 2020, **35**, 1080–1099.
7 Z. Zhang, H. J. Yu, S. Wu, H. Huang, L. P. Si, H. Y. Liu, L. Shi and H. T. Zhang, Synthesis, characterization, and photodynamic therapy activity of 5,10,15,20-Tetrakis(carboxyl)porphyrin, *Bioorg. Med. Chem.*, 2019, **27**, 2598–2608.
8 J. Elms, P. N. Beckett, P. Griffin and A. D. Curran, Mechanisms of isocyanate sensitisation. An *in vitro* approach, *Toxicol. in Vitro*, 2001, **15**, 631.
9 V. Milacic and Q. P. Dou, The tumor proteasome as a novel target for gold(III) complexes: Implications for breast cancer therapy, *Coord. Chem. Rev.*, 2009, **19**, 398–403.
10 A. D. Lammer, M. E. Cook and J. L. Sessler, Synthesis and anti-cancer activities of a water soluble gold(III) porphyrin, *J. Porphyrins Phthalocyanines*, 2015, **19**, 398–403.
11 S. Shamaila, N. Zafar, S. Riaz, R. Sharif, J. Nazir and S. Naseem, Gold nanoparticles: An efficient antimicrobial agent against enteric bacterial human pathogen, *Nanomaterials*, 2016, **6**, 71.
12 N. Kutsevol, Y. Harahuts, I. Shton, T. Borikun, D. Storchai, N. Lukianova and V. Chekhun, In vitro study of toxicity of hybrid gold-polymer composites, *Mol. Cryst. Liq. Cryst.*, 2018, **671**, 1–8.
13 H. Yu, Y. Peng, Y. Yang and Z. Y. Li, Plasmon-enhanced light-matter interactions and applications, *npj Comput. Mater.*, 2019, **45**, 1–14.
14 J. J. Baumberg, J. Aizpurua, M. H. Mikkelsen and D. R. Smith, Extreme nanophotonics from ultrathin metallic gaps, *Nat. Mater.*, 2019, **18**, 668–678.
15 W. Hou and S. B. Cronin, A review of surface plasmon resonance-enhanced photocatalysis, *Adv. Funct. Mater.*, 2013, **23**, 1612–1619.

16 Y. Zhang, K. Aslan, M. J. R. Previte and C. D. Geddes, Metal-enhanced singlet oxygen generation: A consequence of plasmon enhanced triplet yields, *J. Fluoresc.*, 2007, **17**, 345–349.

17 N. Macia, V. Kabanov, M. Côté-Cyr and B. Heyne, Roles of near and Far Fields in Plasmon-Enhanced Singlet Oxygen Production, *J. Phys. Chem. Lett.*, 2019, **10**, 3654–3660.

18 N. Macia, V. Kabanov and B. Heyne, Rationalizing the Plasmonic Contributions to the Enhancement of Singlet Oxygen Production, *J. Phys. Chem. C*, 2020, **124**, 3768–3777.

19 O. Planas, N. Macia, M. Agut, S. Nonell and B. Heyne, Distance-Dependent Plasmon-Enhanced Singlet Oxygen Production and Emission for Bacterial Inactivation, *J. Am. Chem. Soc.*, 2016, **138**, 2762–2768.

20 M. Tavakkoli Yaraki, S. Daqiqeh Rezaei and Y. N. Tan, Simulation guided design of silver nanostructures for plasmon-enhanced fluorescence, singlet oxygen generation and SERS applications, *Phys. Chem. Chem. Phys.*, 2020, **22**, 5673–5687.

21 M. M. Mohamed, S. A. Fouad, H. A. Elshoky, G. M. Mohammed and T. A. Salaheldin, Antibacterial effect of gold nanoparticles against Corynebacterium pseudotuberculosis, *Int. J. Vet. Sci. Med.*, 2017, **5**, 23–29.

22 O. A. Yeshchenko, N. V. Kutsevol and A. P. Naumenko, Light-Induced Heating of Gold Nanoparticles in Colloidal Solution: Dependence on Detuning from Surface Plasmon Resonance, *Plasmonics*, 2016, **11**, 345–350.

23 O. A. Yeshchenko and V. V. Kozachenko, Light-induced heating of dense 2D ensemble of gold nanoparticles: dependence on detuning from surface plasmon resonance, *J. Nanoparticle Res.*, 2015, **17**, 296.

24 Y. I. Harahuts, V. A. Pavlov, E. V. Mokrinskaya, N. G. Chuprina, N. A. Davidenko, A. P. Naumenko, T. M. Bezugla and N. V. Kutsevol, The study of Au sol synthesized in uncharged and charged star-like copolymers under light irradiation, *Funct. Mater.*, 2019, **4**, 723–728.

25 N. Kutsevol, Y. Kuziv, T. Bezugla, P. Virych, A. Marynin, T. Borikun, N. Lukianova, P. Virych and V. Chekhun, Application of new multicomponent nanosystems for overcoming doxorubicin resistance in breast cancer therapy, *Appl. Nanosci.*, 2021, DOI: 10.1007/s13204-020-01653-y.

26 N. Millenbaugh, J. Baskin, M. DeSilva, W. Elliott and R. Glickman, Photothermal killing of Staphylococcus aureus using antibody-targeted gold nanoparticles, *Int. J. Nanomed.*, 2015, **10**, 1953–1960.

27 Z. Z. J. Lim, J. E. J. Li, C. T. Ng, L. Y. L. Yung and B. H. Bay, Gold nanoparticles in cancer therapy, *Acta Pharmacol. Sin.*, 2011, **32**, 983–990.

28 G. Von Maltzahn, J. H. Park, K. Y. Lin, N. Singh, C. Schwöppe, R. Mesters, W. E. Berdel, E. Ruoslahti, M. J. Sailor and S. N. Bhatia, Nanoparticles that communicate *in vivo* to amplify tumour targeting, *Nat. Mater.*, 2011, **10**, 545–552.

29 A. Karabasz, M. Bzowska and K. Szczepanowicz, Biomedical applications of multifunctional polymeric nanocarriers: A review of current literature, *Int. J. Nanomed.*, 2020, **15**, 8673–8696.

30 N. V. Kutsevol, V. A. Chumachenko, I. I. Harahuts and A. I. Marinin, Aging process of gold nanoparticles synthesized *in situ* in water solutions of polyacrylamides, Chemical Engineering of Polymers. *Production of Functional and Flexible Materials*, 2017, pp. 119–129.

31 L. Bulavin, N. Kutsevol, V. Chumachenko, D. Soloviov, A. Kuklin and A. Marynin, SAXS Combined with UV-vis Spectroscopy and QELS: Accurate Characterization of Silver Sols Synthesized in Polymer Matrices, *Nanoscale Res. Lett.*, 2016, **11**, 35.

32 V. Chumachenko, N. Kutsevol, Y. Harahuts, M. Rawiso, A. Marinin and L. Bulavin, Star-like dextran-graft-pnipam copolymers. Effect of internal molecular structure on the phase transition, *J. Mol. Liq.*, 2017, **235**, 77–82.

33 S. Deng, M. R. Gigliobianco, R. Censi and P. Di Martino, Polymeric nanocapsules as nanotechnological alternative for drug delivery system: Current status, challenges and opportunities, *Nanomaterials*, 2020, **10**, 847.

34 V. A. Chumachenko, I. O. Shton, E. D. Shishko, N. V. Kutsevol, A. I. Marinin and N. F. Gamaleia, in *Nanophysics, Nanophotonics, Surface Studies, and Applications, Springer Proceedings in Physics series*, ed. O. Fesenko and L. Yatsenko, 2016, pp. 379–390.

35 N. Kutsevol, P. Virych, O. Nadtoka, P. Virych and V. Krysa, Synthesis of polymeric hydrogels incorporating chlorhexidine as potential antibacterial wound dressings, *Mol. Cryst. Liq. Cryst.*, 2021, **720**, 65.

36 O. Nadtoka, P. Virych, T. Bezugla, V. Doroschuk, S. Lelyushok, V. Pavlenko, O. Yeshchenko and N. Kutsevol, Antibacterial hybrid hydrogels loaded with nano silver, *Appl. Nanosci.*, 2021, DOI: 10.1007/s13204-021-01706-w.

37 P. Virych, O. Nadtoka, V. Doroschuk, S. Lelyushok, V. Chumachenko, T. Bezugla and N. Kutsevol, Cefuroxime-loaded hydrogels for prevention and treatment of bacterial contamination of open wounds, *J. Polym. Sci.*, 2021, **2021**, 4935642.

38 P. Virych, O. Nadtoka, P. Virych, V. Martynyuk and N. Kutsevol, Biochemical and medical studies of bactericidal activity of hydrogels with silver nanoparticles, *Interdiscip. descr. complex syst.*, 2020, **16**, 47–59.

39 N. Kutsevol, T. Bezugla, M. Bezuglyi and M. Rawiso, Branched dextran-graft-polyacrylamide copolymers as perspective materials for nanotechnology, *Macromol. Symp.*, 2012, **317–318**, 82–90.

40 N. Kutsevol, M. Bezuglyi, T. Bezugla and M. Rawiso, Star-like dextran-graft-(polyacrylamide-co-polyacrylic acid) copolymers, *Macromol. Symp.*, 2014, **335**, 12–16.

41 N. Kutsevol, V. Chumachenko, M. Rawiso and A. Shyichuk, Green synthesis of silver nanoparticles using dextran-graft-polyacrylamide as template, *Micro Nano Lett.*, 2016, **11**, 256–259.

42 X. Yuan, Z. Liu, Y. Wang, Y. Xu, W. Zhang and T. Mu, The non-negative truncated singular value decomposition for adaptive sampling of particle size distribution in dynamic

light scattering inversion, *J. Quant. Spectrosc. Radiat. Transfer*, 2020, **246**, 106917.

43 D. F. Marsh and L. M. Mink, Microscale synthesis and electronic absorption spectroscopy of tetraphenylporphyrin H2(TPP) and metalloporphyrins ZnII(TPP) and NiII(TPP), *J. Chem. Educ.*, 1996, **73**, 1181.

44 J. P. Strachan, S. Gentemann, J. Seth, W. A. Kalsbeck, J. S. Lindsey, D. Holten and D. F. Bocian, Effects of orbital ordering on electronic communication in multiporphyrin arrays, *J. Am. Chem. Soc.*, 1997, **119**, 11191–11201.

45 A. Harriman, Luminescence of porphyrins and metalloporphyrins. Part 1. - Zinc(II), nickel(II) and manganese(II) porphyrins, *J. Chem. Soc., Faraday Trans. 1*, 1980, **6**, 1978–1985.

46 K. A. Nguyen, P. N. Day, R. Pachter, S. Tretiak, V. Chernyak and S. Mukamel, Analysis of absorption spectra of zinc porphyrin, zinc meso-tetraphenylporphyrin, and halogenated derivatives, *J. Phys. Chem. A*, 2002, **106**, 10285–10293.

47 P. Törmö and W. L. Barnes, Strong coupling between surface plasmon polaritons and emitters: A review, *Rep. Prog. Phys.*, 2015, **78**, 013901.

48 A. L. Rodarte and A. R. Tao, Plasmon-exciton coupling between metallic nanoparticles and dye monomers, *J. Phys. Chem. C*, 2017, **121**, 3496–3502.

49 P. Anger, P. Bharadwaj and L. Novotny, Enhancement and quenching of single-molecule fluorescence, *Phys. Rev. Lett.*, 2006, **96**, 113002.

50 O. A. Yeshchenko, P. S. Khort, N. V. Kutsevol, V. M. Prokopets, O. Kapush and V. Dzhagan, Temperature Driven Plasmon-Exciton Coupling in Thermoresponsive Dextran-Graft-PNIPAM/Au Nanoparticle/CdTe Quantum Dots Hybrid Nanosystem, *Plasmonics*, 2021, **16**, 1137–1150.

51 E. M. Roller, C. Argyropoulos, A. Högele, T. Liedl and M. Pilo-Pais, Plasmon-exciton coupling using DNA templates, *Nano Lett.*, 2016, **16**, 5962–5966.

52 A. I. Dolinnyi, Nanometric rulers based on plasmon coupling in pairs of gold nanoparticles, *J. Phys. Chem. C*, 2015, **119**, 4990–5001.

53 Q. Su, C. Jiang, D. Gou and Y. Long, Surface Plasmon-Assisted Fluorescence Enhancing and Quenching: From Theory to Application, *ACS Appl. Bio Mater.*, 2021, **4**, 4684–4705.

54 I. Medintz and N. Hildebrandt, *FRET - Förster Resonance Energy Transfer: From Theory to Applications*, Wiley-VCH Verlag, 2013.

55 S. Brown, J. P. Santa Maria and S. Walker, Wall teichoic acids of gram-positive bacteria, *Annu. Rev. Microbiol.*, 2013, **67**, 313–336.

56 B. Gottenbos, D. W. Grijpma, H. C. Van Der Mei, J. Feijen and H. J. Busscher, Antimicrobial effects of positively charged surfaces on adhering Gram-positive and Gram-negative bacteria, *J. Antimicrob. Chemother.*, 2001, **48**, 7–13.

57 G. V. Vimbela, S. M. Ngo, C. Fraze, L. Yang and D. A. Stout, Antibacterial properties and toxicity from metallic nanomaterials, *Int. J. Nanomed.*, 2017, **12**, 3941–3965.